ELSEVIER

Biophysical Chemistry 86 (2000) 37–47

Biophysical Chemistry

www.elsevier.nl/locate/bpc

DNA, RNA and hybrid RNA–DNA oligomers of identical sequence: structural and dynamic differences

Flavia Barone[a], Luciano Cellai[b], Mirella Matzeu[a], Filomena Mazzei[a,*], Francesco Pedone[c]

[a] *Laboratorio di Fisica, Istituto Superiore di Sanità, Viale Regina Elena, 299, 00161 Rome, Italy*
[b] *Istituto di Strutturistica Chimica, CNR, Monterotondo, Rome, Italy*
[c] *Istituto di Genetica e Biologia Molecolare and INFM, Università La Sapienza, Rome, Italy*

Received 27 January 2000; received in revised form 7 April 2000; accepted 7 April 2000

Abstract

A 27-mer sequence was synthesised as DNA duplex (DD), RNA duplex (RR), and RNA–DNA (RD) hybrid in order to characterise their structural and dynamic features. The hydrodynamic radius (R_h) and the rise (b) values of the three samples were consistent with the conformations predicted by CD analysis. The value of the torsional constant (α) of the samples containing RNA was approximately twice that of the DD sample and followed the order: DD < RD < RR. The same order was observed in the thermodynamic stability and in the reduction of the electrophoretic mobility. γ-Ray footprinting analysis was carried out to resolve the individual strand conformation in the hybrid. The RNA strand preserved its conformation, while the DNA strand showed local deformations mainly at TA and TG steps.

Keywords: FPA; RNA–DNA hybrid; γ-Ray footprinting; Nucleic acid conformation; Nucleic acid thermodynamics

1. Introduction

DNA and RNA chains associate in many biological processes with either homologous or heterologous strands to produce DNA–DNA (DD), RNA–RNA (RR) and RNA–DNA (RD) double helices. Due to their specificity in interacting with proteins and in particular in being differently recognised by nuclease enzymes [1], many studies have been carried out to try to identify the relevant differences in their conformation and thermodynamic properties. More recently, the interest in these studies has increased due to the

* Corresponding author. Tel.: +39-064-990-2612; fax: +39-064-938-7075.
E-mail address: mazzei@iss.it (F. Mazzei).

0301-4622/00/$ - see front matter
PII: S0301-4622(00)00157-5

widespread use of oligonucleotides in antisense strategy. Hybridisation of DNA oligomers with target mRNA, aimed at repressing gene expression, requires detailed information on their structure and stability.

Apart from structural and thermodynamic properties, it is interesting to study the dynamic features of short oligonucleotide duplexes. This approach integrates structural information and gives insight into the conformational adaptability of nucleic acids to interact with other macromolecules.

The fluorescence polarisation anisotropy (FPA) technique is a useful tool for studying nucleic acid dynamics. FPA measurements follow the fluorescence decay of dye bound to the molecules as related to its motion in solution. These measurements, performed on duplexes of sizes ranging from 10 to up to 50 bp modelled as rigid cylinders, furnish the hydrodynamic radius and the torsional constant values of the macromolecules [2,3]. Recently this approach has been used to correlate changes in the dynamic properties and in particular in the torsional fluctuations due to the presence of defects in DNA duplexes [4], to the effects of the DNA sequence [5] and to strandedness [6]. This analysis can be extended to RNA duplexes, which are usually found in the A conformation.

An intriguing problem is represented by the structural and dynamic properties of the hybrid RNA–DNA helices, also in relation to RNase enzyme activity. Discussion is still open about whether the cause of the structural recognition of this enzyme is related to the minor groove width or a more general conformational adaptability [7,8].

In this paper we studied the dynamics of deoxy- or ribo-oligonucleotide duplexes and of a hybrid sample; all had the same base pair numbers and sequence and were formed by the association of a purine-rich and a pyrimidine-rich strand.

Structural information, derived from circular dichroism and electrophoresis analysis, and thermodynamic data were obtained to characterise the different nucleic acid forms more effectively. In agreement with other authors [9–11] we showed that the hybrid duplex conformation has an intermediate character between A and B forms. These measurements generally produce average values of the observed parameters. In order to investigate the individual character of the RNA and DNA strand in the hybrid samples we used γ-ray footprinting technique. These experiments provided insight into the nucleic acid's fine three-dimensional structure and made it possible to analyse the accessibility of the sugar phosphate backbone to the attack of hydroxyl radicals [5,12–14].

2. Materials and methods

2.1. Materials

Both DNA and RNA oligomers were prepared by solid-phase automatic synthesis on an ABI 392 apparatus, according to the cyanoethylphosphoramidite chemistry, at the 1-μmol scale. The samples were purified by HPLC on a column of Pure DNA Dynamax-300 A (Rainin, Woburn, MA, USA), 5 μmol, 21.4×50.0 mm, by a gradient of acetonitrile in sterile triethylammonium acetate, 0.1 M (pH 7).

The oligonucleotide purity was checked by denaturing polyacrylamide gel electrophoresis (PAGE) and usually the samples to be used contained less than 2% of lower molecular weight fragments.

Samples were dissolved at a concentration of 1 mg ml^{-1} in deionised water. DNA and RNA single strand concentration was calculated according to Cantor et al. [15] and Gray et al. [16], respectively. The annealing of the DD and RR duplex samples and of the two possible hybrid forms was performed at a 1:1 molar ratio in the desired buffer, by heating solutions to 90°C and cooling them slowly to 4°C. For spectrophotometric and fluorescence analysis the buffer used was 10 mM Tris–HCl, 50 mM NaCl, 1 mM Na_2EDTA (pH 7.2). Footprinting experiments were performed in 10 mM Na phosphate buffer at pH 7.2. Complete annealing of the samples was checked by PAGE in 45 mM Tris–borate, 1 mM Na_2EDTA, TBE buffer (pH 8) at 4°C, 80 V for 17 h. The hybrid with the RNA pyrimidine-rich

5′GAAGAATAAGAATAACAAGCAGAAGAG3′
3′CTTCTTATTCTTATTGTTCGTCTTCTC5′(DD)

5′gaagaauaagaauaacaagcagaagag3′
3′CTTCTTATTCTTATTGTTCGTCTTCTC5′(RD)

5′gaagaauaagaauaacaagcagaagag3′
3′cuucuuauucuuauuguucgucuucuc5′(RR)

Fig. 1. Sequences of DNA and RNA homologous and heterologous duplexes.

strand, especially in the buffer used in footprinting experiments, was very unstable at low temperatures. The hybrid with the RNA purine-rich strand formed a stable duplex and was used throughout this work.

The sequence of the samples is shown in Fig. 1.

2.2. Fluorescence dynamic measurements

The dynamics of RNA and DNA duplexes was followed by monitoring the fluorescence polarisation anisotropy decay (FPA) of the ethidium bromide (EB) dye bound to homologous and heterologous duplexes. A frequency domain fluorometer (K2-ISS, Urbana, IL, USA) was used, exciting the dye fluorescence emission with the 514-nm 0.5-W output of a Coherent Innova 90C argon laser. The modulation ratio of the excitation light was always in the range of 60–70% and the detection cross-correlation frequency was 80 Hz. A detailed report of the experimental setup is given elsewhere [6].

The duplexes, at a concentration of 0.6 mM oligonucleotide, were dissolved in the buffer and EB added at a ratio of 1 mol of EB per 300 bp, in order to avoid energy transfer phenomena. Thermostatation was allowed by a circulating water bath (Haake K15) and the temperature of the block containing the sample cuvette was continuously monitored during the measurements in the range 4–30°C with an Ellab probe.

Lifetime determination between 4 and 30°C was carried out in all the samples at each temperature before performing the corresponding anisotropy measurement. For the lifetime measurements, 10 frequencies logarithmically spaced in the 2–40 MHz interval were acquired. The excitation polariser was set at 36° with respect to vertical polarisation of the laser and polystyrene latex was used as the reference. The data were analysed with the ISS fluorometer software running on a PC, using the lifetime value of free ethidium equal to 1.7 ns. The lifetime vs. temperature data were fitted by a linear regression and this dependence was accounted for in the following FPA data analysis.

Anisotropy data were acquired at 20 frequencies in the 2–40 MHz interval with the excitation polariser kept fixed at 0° (i.e. vertical) and the emission polariser automatically rotated at 0 and 90° for each acquisition. The error for phase and modulation ratio was 0.2° and 0.004, respectively, amounting to $\approx 1\%$ of the signal.

In the frequency domain, the quantities usually measured to characterise the fluorescence polarisation anisotropy decay are the difference between the phase angles (Φ) of the two components, parallel and perpendicular, with respect to the excitation beam, and the demodulation (M) ratio, according to:

$$\Delta\Phi = \Phi_{\perp} - \Phi_{\parallel}$$

$$\Delta\Lambda = M_{\parallel}/M_{\perp}$$

These quantities are related to the time decay of the fluorescence intensity (I) as measured when the relative orientation of the excitation polariser and the emission analyser are parallel ($I_{\parallel}$) or orthogonal ($I_{\perp}$), by means of Laplace transforms.

The Laplace transforms

$$f_{\mathrm{p}}(\omega) = \int_0^{\infty} \mathrm{d}t I_{\mathrm{p}}(t) e^{i\omega t} = L(I_{\mathrm{p}})(i\omega)$$

where $\mathrm{p} = \parallel$ or $\mathrm{p} = \perp$ were computed and combined as:

$$\Delta(\omega) = \mathrm{arctg}\frac{\mathrm{Im}(f_{\perp})\mathrm{Re}(f_{\parallel}) - \mathrm{Im}(f_{\perp})\mathrm{Re}(f_{\parallel})}{\mathrm{Re}(f_{\perp})\mathrm{Re}(f_{\parallel}) + \mathrm{Im}(f_{\perp})\mathrm{Im}(f_{\parallel})}$$

and:

$$\Lambda(\omega) = |f_{\perp}(\omega)|/|f_{\parallel}(\omega)|$$

The decay of fluorescence anisotropy is well described by the product of correlation functions, which are referred to as the motions of the nucleic acids themselves:

$$r(t) = \frac{I_{\parallel} - I_{\perp}}{I_{I_{\parallel}} + 2I_{\perp}} = r_0 \sum_{n=-2}^{2} A_n(t) C_n(t) F_n(t)$$

where r_0 is the EB limiting anisotropy value, which is usually found to be equal to 0.36 [17]. A_n are the internal correlation functions which are fully described by trigonometric functions of the angle θ formed by the EB dipole and the helical axis, which has been assumed to be equal to 70.5° [18]. $C_n(t)$ and $F_n(t)$ are the torsional and the bending correlation functions, respectively. All the correlation functions are fully described elsewhere [5].

For a straight fragment, the rotational diffusion coefficients can be computed by assuming that the DNA behaves as a straight cylinder of length L and radius R, i.e. [19]:

$$D_{\parallel} = k_B T / \left[(3.8441) \pi \eta L R^2 (1 + \delta_{\parallel}) \right];$$

$$D_{\perp} = 3 k_B T (\ln p + \delta_{\perp}) / \pi \eta L^3$$

$$\delta_{\parallel} = (0.677/p) - \left(0.183/p^2\right);$$

$$\delta_{\perp} = -0.662 + (0.917/p) - 0.05/p^2$$

where $p = (L/2R)$, T is the absolute temperature and η is the solution viscosity.

Phase differences and demodulation ratios in the FPA measurements were fitted with a Vax station in order to obtain the hydrodynamic parameters. During the fitting procedure the torsional constant α, the hydrodynamic radius R_h and the rise b were the free parameters.

2.3. Circular dichroism and UV melting

Circular dichroism (CD) spectra were recorded by means of a Jasco J710 spectropolarimeter between 200 and 320 nm, with a scanning rate of 10 nm min^{-1}. The spectral resolution was 0.2 nm and the band width 1 nm. The samples [approx. 2.5 μM of oligonucleotide in 10 mM Tris HCl, 50 mM NaCl, 1 mM Na_2EDTA (pH 7.2)] were thermostated with a Peltier-type temperature control system (Jasco, Model PTC-348 WI) at 10°C, in 1-cm path length cells. A nitrogen stream was flushed on the cuvette wall to avoid water condensation.

UV absorption changes at 260 nm were followed by means of a Cary 3 UV/VIS spectrophotometer. The temperature was controlled by a Peltier device and raised at a rate of 0.5°C min^{-1}. Absorbance values of the samples were corrected for thermal expansion of the water and normalised at one value of optical density at the lower temperature. Thermodynamic analysis was performed according to Breslauer [20]. Hyperchromicity was calculated as percent change of absorbance between 4 and 80°C.

2.4. Gel electrophoresis

Samples were electrophoresed on non-denaturing 15% polyacrylamide gels in TBE buffer at 4°C, 80 V for 17 h. After the run DNA bands were visualised by staining with ethidium bromide and photographed under ultraviolet light. The band migration was measured by densitometric analysis of the negative film (ULTROSCAN XL, Pharmacia LKB).

2.5. γ-Ray footprinting

DNA and RNA single-stranded oligomers purified by HPLC were further purified by denaturing PAGE. The fragments, eluted by an overnight incubation in deionised water at 37°C, were ethanol-precipitated with 3 M NaAcetate (pH 5.2). The 5′(CTCTTCTGCTTGTTATTCTTATTCTTC)3′ DNA, the 5′(GAAGAATAAGAATAACAAGCAGAAGAG)3′ DNA and the 5′(gaagaauaagaauaacaagcagaagag)3′ RNA oligomers were 5′-end labelled by incubation with [γ-^{32}P]ATP (Dupont) and the T4 polynucleotide kinase enzyme (Boehringer-Mannheim). After purification through a Sephadex G-25 column, the 5′-end labelled oligomers were annealed in 10 mM sodium phosphate buffer (pH 7.2) with an

excess of unlabeled complementary strands in order to obtain the following duplexes: DD*, RD*, D*D, R*D, R*R, where the * symbol indicates the labelled strand. Complete annealing was checked by 15% PAGE analysis in recirculating TBE buffer at 80 V and 4°C for 17 h.

Annealed samples were irradiated at a concentration of approximately 40 nM of oligonucleotide. The irradiation was performed in an ice-water bath in a GammaCell 220 (AECL), equipped with a ^{60}Co source, at the dose of approximately 50 Gy. The dose rate was approximately 5 Gy min^{-1}.

Irradiated samples were run on 20% denaturing polyacrylamide sequencing gels ($20 \times 40 \times 0.04$ cm), containing 7 M urea in TBE buffer [21]. The identification of guanine and adenine bases on sequencing gels was performed according to Negri et al. [22]. A short- and a long-run gel were run at 28 W, for 2 and 4 h, respectively, in order to obtain a better resolution of the lower and upper part of the gel. Fixed gels were dried at 60°C for 10 min and autoradiographed using a Kodak X-OMAT S film with intensifying screens.

The densitometric analysis of the autoradiographs was performed by an ULTROSCAN XL (Pharmacia LKB) laser densitometer. The area of each band was evaluated using the public domain NIH Image program as already reported [5]. In the analysis, the first and the last two or three bands were omitted from area integration, considered of too high and too low intensity, respectively. The maximum calculated error, deriving from both measurement and analysis reproducibility, was equal to $\pm 10\%$.

3. Results and discussion

3.1. DNA and RNA dynamics

Lifetime values show very large differences among homologous DNA, RNA and hybrid duplexes. As Table 1 shows, the lifetime values of the bound EB at 0°C span from 23.6 ns in DNA to 29.8 ns in RNA samples. An intermediate situation was found for the hybrid duplex. These results suggest differences in the geometry of the intercalation site of the EB, which exhibits greater affinity for RNA-containing duplexes.

Table 1
Lifetime values for DNA and RNA samples and dependence on temperature

Sample	τ_{bT} (ns)
DD	23.6–0.05 T
RD	27.4–0.05 T
RR	29.8–0.05 T

The lifetime values decrease with temperature with the same slope in the three samples (Table 1). This effect may be due to the increased exposure of the intercalated EB to the solvent molecules, following the increase in thermal motion, and to the onset of base-stacking decrease.

More information on base stacking and on the hydrodynamic properties of these molecules can be drawn from FPA measurements, through the

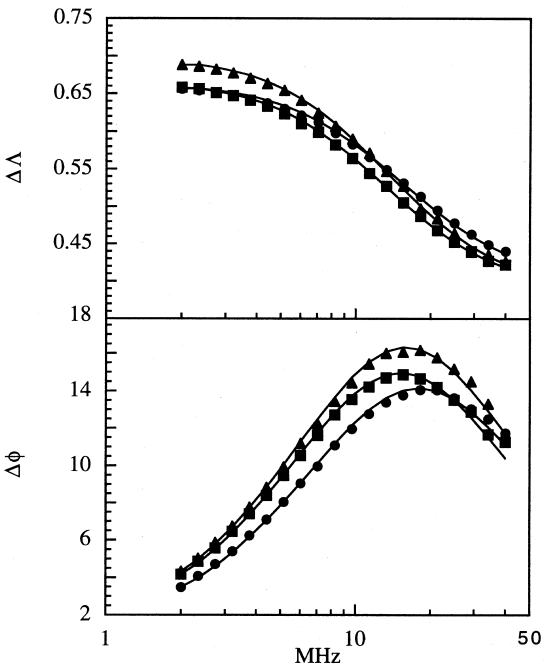

Fig. 2. FPA measurements: demodulation ratios (top) and phase differences (bottom) of DNA, RNA and hybrid duplexes as a function of the modulation frequency at 10°C. Circle, DD; square, RD; and triangle, RR. The samples (0.6 mM of oligonucleotide) were in 10 mM Tris–HCl, 50 mM NaCl, 1 mM Na_2 EDTA (pH 7.2).

Table 2
Main parameters derived from FPA analysis

Sample	α (10^{-19}J)	R_h (nm)	b (nm)	$\Delta\xi$ (°)	χ^2
DD	7.2 ± 0.2	1.07 ± 0.03	0.33 ± 0.01	4.21 ± 0.02	1.04
RD	13.2 ± 0.3	1.27 ± 0.03	0.28 ± 0.01	3.12 ± 0.02	1.02
RR	14.3 ± 0.3	1.28 ± 0.03	0.27 ± 0.01	2.99 ± 0.02	1.00

study of the decay of the fluorescence polarisation anisotropy of the bound EB dye.

Fig. 2 shows the phase difference and demodulation ratio of DD, RD and RR samples as a function of the modulation frequency. The RR duplex shows the largest differences. The differential phase peak in the RR duplex and the region of increased demodulation are shifted towards lower frequencies. Both these experimental findings are consistent with a reduction in the rotational relaxation time and thus, a slower motion of the sample. The hybrid duplex behaves similarly to the RR duplex.

In Table 2 the torsional rigidity constant (α), the hydrodynamic radius (R_h), the rise (b), and the rms fluctuation angles per base pair ($\Delta\xi$) at $10 \pm 1°$ are reported. $\Delta\xi$ is defined as: $\Delta\xi = \sqrt{kT/\alpha}$, where k is the Boltzman constant and T the absolute temperature. As Table 2 shows, duplexes containing RNA are approximately twice as rigid as the corresponding DNA sample.

We recently observed a variation of approximately 10% in the torsional constant in two 27-mer DNA duplexes with the same base composition and different sequence [5]. We attributed these changes mainly to stacking interaction between neighbouring base pairs. In this case, the RR and DD samples of identical sequence also differ in the sugar structure, so the large differences observed in rigidity can be due to variations both in the base–base interaction and in the sugar backbone structure. In the hybrid sample, there are only two T/U substitutions with respect to the DD sample, while the rigidity constant is very similar to that of the RNA duplex, which contains another 16 T/U substitutions. The comparison of these two samples indicates that base substitution affects the torsional constant less than the backbone modification.

The calculated radius as well as the rise in the DD sample are characteristic of the B form, while the values in the RR and RD duplexes are indicative of A-like conformations. Taking into account the rise value shown in Table 2, a length value reduction from 8.9 nm in the DD duplex to 7.3 nm in the RR duplex and to 7.6 nm in the RD sample was calculated.

Table 3 shows the rotational diffusion coefficients of the three samples at 10°C. A reduction in the asymmetry of the RD and RR samples of approximately 60–70% was found with respect to the DD duplex, as indicated by the decrease in the $D_{\parallel}/D_{\perp}$ ratio. The $D_{\parallel}$ value of the hybrid is lower, possibly due to a shape deviating from the classic cylindrical model.

Fig. 3 reports the behaviour of the torsional constant with temperature. The temperature dependence of the duplex torsional constant is complex and mainly related to interactions such as hydration forces, hydrogen bonds, base stacking and to the structure of the sugar phosphate backbone. As the temperature increases toward the melting point, the α values of the studied samples converge to the same value of approximately 2.5×10^{-19} J at 60°C, when empirically fitted with an exponential law. Corresponding to this value, a rms fluctuation angle of 7.7° per bp is derived, i.e. an increase of approximately twofold in the $\Delta\xi$ value is obtained in the temperature range

Table 3
Rotational diffusion coefficients of RNA and DNA samples at 10°C

Sample	$D_{\parallel}$ (MHz)	$D_{\perp}$ (MHz)	$D_{\parallel}/D_{\perp}$
DD	20.9 ± 1.2	3.1 ± 0.2	6.7
RD	16.7 ± 1.0	3.8 ± 0.2	4.4
RR	18.9 ± 1.1	4.6 ± 0.3	4.1

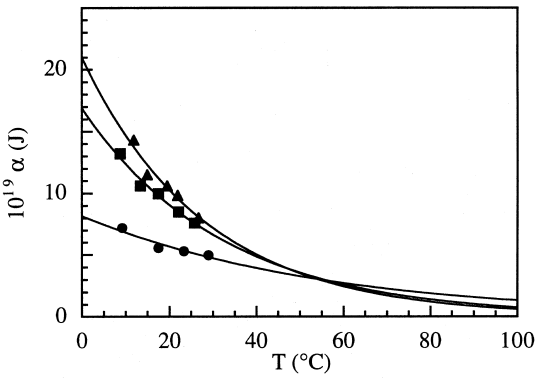

Fig. 3. Torsional rigidity constant of DNA, RNA and hybrid duplexes as a function of the temperature. Circle, DD; square, RD; and triangle, RR. The samples (0.6 mM of oligonucleotide) were in 10 mM Tris–HCl, 50 mM NaCl, 1 mM Na_2 EDTA (pH 7.2).

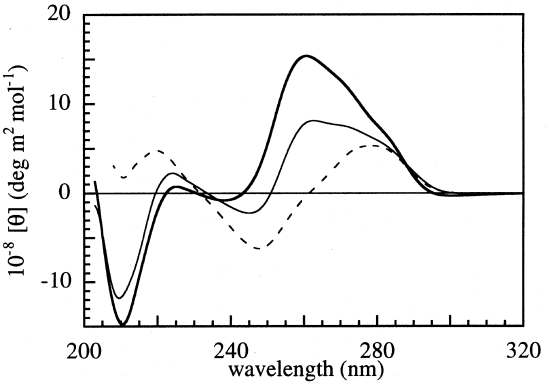

Fig. 4. Circular dichroism spectra at 10°C of DNA, RNA and hybrid duplexes. Bold line, RR; thin line, RD; and dashed line, DD. The samples (2.5 μM of oligonucleotide) were in 10 mM Tris–HCl, 50 mM NaCl, 1 mM Na_2 EDTA (pH 7.2).

between 4 and 60°C. It should be observed that this increase in the twist angle fluctuations with temperature is consistent with the onset of the destabilisation of the double helix. Better knowledge of the temperature dependence law could be useful to estimate relative thermodynamic stability.

3.2. Circular dichroism spectra

In order to support the results of the dynamic measurements and in particular the conformations suggested by the structural parameters derived from FPA analysis, we performed CD spectra.

Circular dichroism spectra between 200 and 320 nm were recorded at 10°C, at which temperature all duplexes are thermally stable (Fig. 4). The DD duplex shows a typical conservative spectrum with two equally pronounced positive and negative peaks at approximately 280 and 250 nm. The RR duplex clearly shows a non-conservative spectrum with a positive maximum at 265 nm, while a negative band is present with a minimum at 210 nm. The recorded spectra are characteristic of the B and A nucleic acid conformations, respectively.

The hybrid RD sample shows a CD spectrum very similar to that of the A form. In fact, the spectrum appears to be non-conservative in shape with a negative band at lower wavelength as well. Thus, the hybrid conformation is very similar to that of the RR duplex, in good agreement with some literature data obtained in a RD sample, with a purine-rich RNA strand [9,10].

3.3. Thermodynamic properties

The thermal stability of the DD, RD and RR duplexes was analysed by UV melting experiments and the calculated thermodynamic parameters are shown in Table 4. It is evident

Table 4
Change of enthalpy (ΔH), entropy (ΔS) and free energy at 37°C (ΔG_{37}), melting temperature (T_m) and hyperchromicity (Hyp) of DD, RD and RR duplexes

Sample	ΔH (kJ mol^{-1})	ΔS (kJ mol^{-1} K^{-1})	ΔG_{37} (kJ mol^{-1})	T_m (°C)	Hyp (%)
DD	-613 ± 42	-1.8 ± 0.1	-68 ± 3	55.6 ± 0.5	35.8 ± 1.1
RD	-688 ± 50	-2.0 ± 0.1	-75 ± 4	58.4 ± 0.5	39.9 ± 1.2
RR	-834 ± 59	-2.3 ± 0.2	-100 ± 5	64.7 ± 0.5	41.6 ± 1.2

from the data that the order of stability is DD < RD < RR.

The stability difference between duplexes formed by DNA or RNA strands can be due to the presence of a 2′-OH group in the ribose moiety in RNA and of a C-5 methyl group in thymine moiety of DNA. In purine-rich/pyrimidine-rich RNA or hybrid RNA/DNA duplexes, the absence of the C-5 methyl group is always destabilising, while the presence of the 2′-OH group produces opposing effects, according to the context [23]. In particular it is stabilising in RNA duplexes or in hybrids with a purine-rich RNA strand, but destabilising if the RNA strand is pyrimidine rich. Thus, the net effect of the two contributions to stability depends on the base composition and the structure (RNA or DNA) of the purine-rich or pyrimidine-rich single strands [9,10].

In the hybrid studied in this work, the absence of the C-5 methyl group is expected to have little influence on the thermodynamic (as well as conformational) properties with respect to the DD duplex, as it only involves two U bases in an RNA strand. Therefore, it must be the backbone structure that is mainly responsible for the greater stability compared with the DD sample. The higher enthalpic contribution to the change in free energy at 37°C (ΔG_{37}) in the melting transition indicates an increase in base stacking, which can be correlated to a larger base–base overlap in the A-like form of the hybrid. The entropic contribution is also larger in the hybrid than in the DD sample, according to the larger torsional rigidity observed by FPA measurements and attributed to the structure of the RNA strand backbone. That produces a partial compensation of the increased enthalpic contribution and moderates the net increase of ΔG_{37}. A correlation between the thermodynamic parameters and the torsional constant values, reported in Tables 4 and 2, respectively, is evident.

Hyperchromism of the hybrid duplex has an intermediate value between that of DD and RR, closer to the RNA duplex. This result confirms a more extensive base stacking compared to that of DNA, according to the A-like conformation, also revealed in CD spectrum of the RD samples.

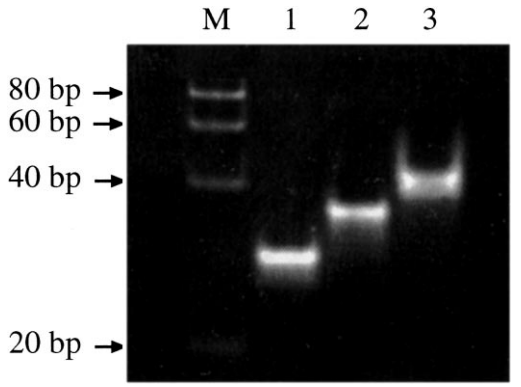

Fig. 5. 15% PAGE of DNA, RNA and hybrid duplexes in 45 mM Tris–Borate, 1 mM Na_2 EDTA, TBE buffer (pH 8) at 4°C, 80 V. Lane M, 20 base pairs (bp) ladder; lane 1, DD; lane 2, RD; and lane 3, RR.

3.4. Electrophoretic mobility evaluation

As Fig. 5 shows, the electrophoretic mobility of the samples is progressively reduced in the order DD < RD < RR according to their mass, i.e. 16 706, 17 034, and 17 206, respectively. This behaviour is in agreement with previous results obtained on similar samples of various length and composition [10,24,25]. However, the gel mobility of the samples containing RNA is still less than expected based on the true mass values. In fact, the RNA duplex and the hybrid sample migrate like DNA duplexes of approximately 25 400 and 21 800 Da, respectively (Fig. 5).

In a non-denaturing gel, samples migrate with an apparent molecular weight which is related to the true molecular weight, the shape and the charge. In this study, all duplexes have the same number of bases and the molecular weight differences are essentially due, as already noted, to the presence of ribose instead of deoxyribose and to the T/U substitution. Relevant differences in shape, in particular in the hydrodynamic volume, could also contribute to the reduced mobility of duplexes containing RNA. This hypothesis agrees with the FPA results, previously shown in Table 2, from which an overall increase in the hydrodynamic volume may be evaluated for the RR and RD duplexes with respect to the DD sample.

As far as the RD sample is concerned, it is

evident that the hybrid sample migrates closer to the RR duplex. This result agrees with the findings of Lesnik and Freier [10] who showed that hybrids with a high content of pyrimidine (greater than 70%) on the DNA strand, as in our case, migrate closer to the RNA homologous duplexes, while samples with a lower pyrimidine content have a mobility similar to that of DNA samples.

In the RD sample, there was no exact correlation between the electrophoretic migration and the hydrodynamic volume as it can be evaluated from Table 2, possibly due to the rough approximation of the rigid cylinder model, which may have to be further refined. Good correlation was observed between the torsional constant values and the electrophoretic data.

3.5. γ-Ray footprinting analysis

Hydroxyl radical footprinting has proven very useful in the characterisation of the fine structure of nucleic acid fragments. Many studies have been published on the effects of sequence and strandedness on DNA conformation [14,26,27], yet the application to RNA is original, apart from some studies where hydroxyl radicals were produced by chemical methods [28].

The aim of footprinting experiments was to analyse the fine conformation of the three samples (DD, RD, RR) to understand whether individual characteristic conformations are possible in the DNA and RNA strand of the hybrid sample, as suggested by NMR studies [7].

In DNA, different kinds of damage might be caused by OH radicals produced in solution by γ-ray irradiation. We only looked at the breakage of the sugar phosphate chain (frank strand break). This damage is mainly due to the direct interaction of the hydroxyl radicals with H4′, H5′1 and H5′2 hydrogen atoms of the sugar moiety [29]. The cutting frequency depends mainly on the sequence and the wideness of the minor groove, so that changes in the backbone conformation of the oligonucleotides can be detected.

The labelled RNA purine-rich or the DNA pyrimidine-rich strand was analysed in association with the homologous and the heterologous strand: R*R and R*D, DD* and RD*. The cutting pattern of the RNA purine-rich strand of the R*D sample (Fig. 6a) looks quite similar to that obtained for the same strand in the R*R sample, so that no relevant changes in the RNA backbone conformation seem to occur. In the same figure, the breakage pattern of the DNA purine-rich strand in the D*D sample, which is in the B form, appears very different from the other two profiles.

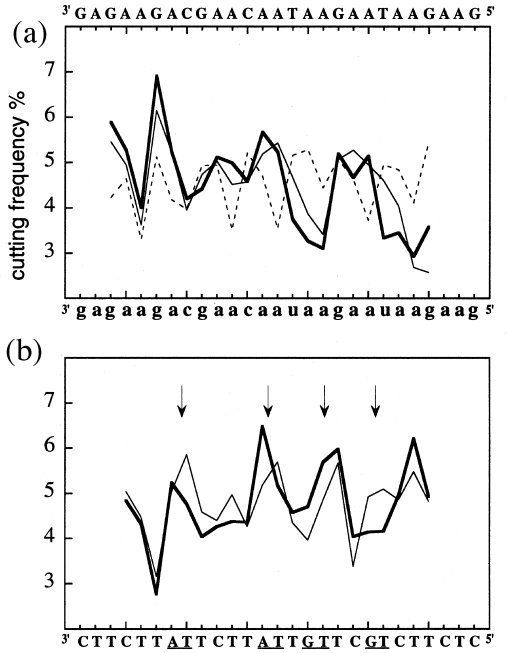

Fig. 6. γ-Ray footprinting analysis. (a) Comparison of the cutting frequency of purine-rich RNA labelled strand in association with the complementary RNA strand (R*R) and with the DNA strand (R*D): bold line, R*R; and thin line, R*D. The cleavage pattern of purine-rich DNA labelled strand (D*D) is also reported as a marker: dashed line, D*D. (b) Comparison of the cutting frequency of pyrimidine-rich DNA labelled strand in association with the complementary RNA strand (DD*) and with the RNA strand (RD*): bold line, DD*; and thin line, RD*. Arrows indicate sites of major changes in cutting probability. The samples [40 nM of oligonucleotide in 10 mM sodium phosphate buffer (pH 7.2)] were irradiated on ice-water bath at the dose of approximately 50 Gy.

Comparison of the backbone accessibility of the DNA pyrimidine-rich strand in the RD* and DD* samples (Fig. 6b) reveals differences at various nucleotide sites. The changes in accessibility to radicals are distributed along the chain and

occur mainly at some selected sites corresponding to interruptions of pyrimidine runs along the chain, i.e. at TA and TG steps. According to the data reported in Fig. 6a, the conformation of the RNA strand in the hybrid duplex, and possibly its length, are almost unchanged. Thus, a deformed B conformation can be stabilised in the DNA strand of the RD hybrid to allow hydrogen bonding between complementary strands. We can hypothesise that the more flexible DNA strand deforms at TA and TG steps, which can be considered as preferential hinge points [30], in order to anneal the hybrid.

4. Conclusions

FPA measurements, performed on duplex samples with either DNA or RNA strands and on a hybrid RNA–DNA sample enabled us to characterise the dynamic properties of samples with the same number of base pairs and composition, but differing in the presence of 2′-OH or 5-methyl on one or both the strands. In particular the three samples had a purine-rich and a pyrimidine-rich strand.

Comparison of experimental and theoretical data predicted by the model [2], as modified by Collini et al. [3], allowed us to evaluate structural parameters such as the torsional constant, the rise and the hydrodynamic radius.

The RNA duplex was found to be twice as rigid as the DNA duplex of identical sequence and base number, i.e. $\alpha = 14.3 \times 10^{-19}$ and 7.2×10^{-19} J at 10°C, respectively. It is characterised by a more compact structure, with reduced asymmetry with respect to the DNA duplex. The rise and the radius of the RR duplex are characteristic of the A-form of nucleic acids ($b = 0.27$ nm, $R_h = 1.28$ nm). The hybrid duplex dynamics resemble that of the RR sample, as the rise and the radius were found equal to 0.28 and 1.27 nm, respectively, and the torsional constant was 13.2×10^{-19} J at 10°C. The observed variations in α enabled us to discriminate between different nucleic acid conformations.

The higher rigidity and the changes in shape associated with the presence of an RNA strand were further confirmed by electrophoretic measurements. The suggestion that the RR and the RD duplexes were in an A-like form was supported by CD analysis. However, the intermediate character of the RD duplex conformation, identified as an A-like form on average, was investigated more thoroughly to explain some features revealed by electrophoretic measurements.

The use of the γ-ray footprinting method allows us to indicate that the RNA conformation in the RD sample is very similar to that assumed in the RR duplex, while the conformation of the DNA strand is altered with respect to the DD form. The different conformation of the two strands may allow local distortions of the double helix mainly at TA and TG steps, which act as hinge points.

Finally, we applied static and dynamic methods and showed that the RR, RD and DD samples have different forms in solution. We could not evaluate minor groove dimension changes, often invoked to explain the variability of enzyme activity. However, we were able to evaluate parameters such as hydrodynamic radius, rise and torsional flexibility, which can be relevant in the interaction with enzymes.

Acknowledgements

We thank G. La Sala for her help in sample purification and C. De Sena for its technical assistance in CD measurements.

References

[1] B. Alberts, D. Bray, J. Lewis, M. Raff, K. Roberts, J.D. Watson, Molecular Biology of the Cell, Garland Pub. Inc, New York, 1994.

[2] S.A. Allison, M. Schurr, Torsion dynamics and depolarization of fluorescence of linear molecules. I. Theory and application to DNA, Chem. Phys. 41 (1979) 35–39.

[3] M. Collini, G. Chirico, G. Baldini, M.E. Bianchi, Conformation of short DNA fragments by modulated fluorescence polarization anisotropy, Biopolymers 36 (1995) 211–225.

[4] F. Barone, F. Cellai, C. Giordano, M. Matzeu, F. Mazzei, F. Pedone, γ-Ray footprinting and fluorescence polarization anisotropy of a 30-mer synthetic DNA fragment with one 2′-deoxy-7-hydro-8-oxoguanosine lesion, Eur. Biophys. J. 28 (2000) 621–628.

[5] F. Barone, M. Matzeu, F. Mazzei, F. Pedone, Structural and dynamical properties of two DNA oligomers with the same base composition and different sequence, Biophys. Chem. 78 (1999) 259–269.
[6] F. Barone, G. Chirico, M. Matzeu, F. Mazzei, F. Pedone, Triple helix oligomer melting measured by fluorescence polarization anisotropy, Eur. Biophys. J. 27 (1998) 137–146.
[7] J.I. Gyi, A.N. Lane, G.L. Conn, T. Brown, Solution structures of DNA.RNA hybrids with purine-rich and pyrimidine-rich strands: comparison with the homologous DNA and RNA duplexes, Biochemistry 37 (1998) 73–80.
[8] T. Szyperski, M. Götte, M. Billeter et al., NMR structure of the chimeric hybrid duplex r(gcaguggc) r(gcca)d(CTGC) comprising the tRNA–DNA junction formed during initiation of HIV-1 reverse transcription, J. Biomol. NMR 13 (1999) 343–355.
[9] L. Ratmeyer, R. Vinayak, Y.Y. Zhong, G. Zon, W.D. Wilson, Sequence specific thermodynamic and structural properties for RNA.DNA duplexes, Biochemistry 33 (1994) 5298–5304.
[10] E.A. Lesnik, S.M. Freier, Relative thermodynamic stability of DNA, RNA and DNA:RNA hybrid duplexes: relationship with base composition and structure, Biochemistry 34 (1995) 10807–10815.
[11] J.I. Gyi, G.L. Conn, A.N. Lane, T. Brown, Comparison of the thermodynamic stabilities and solution conformations of DNA.RNA hybrids containing purine-rich and pyrimidine-rich strands with DNA and RNA duplexes, Biochemistry 35 (1996) 12538–12548.
[12] L. Tartier, V. Michalik, M. Spotheim-Maurizot, A.R. Rahmouni, R. Sabattier, M. Charlier, Radiolytic signature of Z-DNA, Nucleic Acids Res. 22 (1994) 5565–5570.
[13] F. Barone, M. Belli, F. Mazzei, Influence of DNA conformation on radiation-induced single strand breaks, Radiat. Environ. Biophys. 33 (1994) 23–33.
[14] D. Sy, C. Savoye, M. Begusova, V. Michalik, M. Charlier, M. Spotheim-Maurizot, Sequence dependent variations of DNA structure modulate radiation-induced strand breakage, Int. J. Radiat. Biol. 72 (1997) 147–155.
[15] C.R. Cantor, M.M. Warshaw, H. Shapiro, Oligonucleotide interaction. III Circular dichroism studies of the conformation of deoxyoligonucleotides, Biopolymers 9 (1970) 1059–1077.
[16] D.M. Gray, S.H. Hung, K.H. Johnson, Absorption and circular dichroism spectroscopy of nucleic acid duplexes and triplexes, Methods Enzymol. 246 (1995) 19–34.
[17] D. Madge, M. Zappala, W.H. Knox, T.M. Nordlund, Picoseconds fluorescence anisotropy decay in the ethidium/DNA complexes, J. Phys. Chem. 87 (1983) 3286–3288.
[18] J.M. Schurr, Rotational diffusion of deformable macromolecules with mean local cylindrical symmetry, Chem. Phys. 84 (1984) 71–76.
[19] M.M. Tirado, J. Garcia de la Torre, Rotational dynamics of rigid, symmetric top macromolecules. Application to circular cylinders, J. Chem. Phys. 73 (1980) 1986–1993.
[20] K.J. Breslauer, Extracting thermodynamic data from equilibrium melting curves for oligonucleotide order–disorder transitions, in: S. Agraval (Ed.), Methods in Molecular Biology, vol. 26, Humana Press Inc, Totowa, NJ, 1994, pp. 347–372.
[21] J. Sambrook, E.F. Fritsch, T. Maniatis, Molecular Cloning. A Laboratory Manual, Cold Spring Harbor Laboratory Press, Cold Spring Harbor, NY, 1989.
[22] R. Negri, G. Costanzo, E. Di Mauro, A single reaction method for DNA sequence determination, Anal. Biochem. 197 (1991) 389–395.
[23] S. Wang, E.T. Kool, Origins of the large differences in stability of DNA and RNA helices: C-5 methyl and 2′-hydroxyl effects, Biochemistry 34 (1995) 4125–4132.
[24] R.W. Roberts, D.M. Crothers, Stability and properties of double and triple helices: dramatic effects of RNA or DNA backbone composition, Science 8 (1992) 1463–1466.
[25] G.F. Bonifacio, T. Brown, G.L. Conn, A.N. Lane, Comparison of the electrophoretic and hydrodynamic properties of DNA and RNA oligonucleotide duplexes, Biophys. J. 73 (1997) 1532–1538.
[26] V. Isabelle, C. Prévost, M. Spotheim-Maurizot, R. Sabattier, M. Charlier, Radiation induced damages in single- and double-stranded DNA, Int. J. Radiat. Biol. 67 (1995) 169–176.
[27] F. Barone, M. Begusova, E. La Nave, M. Matzeu, F. Mazzei, D. Sy, Radiation damage to triplex DNA induced by γ-rays: footprinting study and Monte Carlo simulation, Int. J. Radiat. Biol. (in press).
[28] M. Götte, G. Mayer, H.J. Gross, H. Heumann, Localization of the active site of HIV-1 reverse transcriptase-associated Rnase H domain on a DNA template using site-specific generated hydroxyl radicals, J. Biol. Chem. 273 (1998) 10139–10146.
[29] C. Von Sonntag, The Chemical Basis of Radiation Biology, Taylor & Francis, London, 1987.
[30] R.P. Ojha, M.M. Dhingra, M.H. Sarma et al., DNA bending and sequence-dependent backbone conformation. NMR and computer experiments, Eur. J. Biochem. 265 (1999) 35–53.